Monthly Notices
of the
ROYAL ASTRONOMICAL SOCIETY

MNRAS **492,** 3742–3752 (2020)
Advance Access publication 2020 January 23

doi:10.1093/mnras/stz3586

The vertical Na–O relation in the bulge globular cluster NGC 6553

C. Muñoz,[1★] S. Villanova,[2] D. Geisler,[2,3,4] C. C. Cortés,[2,5] C. Moni Bidin,[6] R. E. Cohen,[7] I. Saviane,[8] B. Dias,[8,9] B. Tang[10] and F. Mauro[6]

[1]*INAF, Osservatorio Astronomico di Roma, Via Frascati 33, I-00040 Monte porzio Catone (Roma), Italy*
[2]*Departamento de Astronomía, Universidad de Concepción, Casilla 160-C, Concepción, Chile*
[3]*Instituto de Investigación Multidisciplinario en Ciencia y Tecnología, Universidad de La Serena, Avenida Raúl Bitrán S/N, La Serena, Chile*
[4]*Departamento de Astronomía, Facultad de Ciencias, Universidad de La Serena, Av. Juan Cisternas 1200, La Serena, Chile*
[5]*Departamento de Física, Facultad de Ciencias, Universidad del Bío-Bío, Avenida Collao 1202, Casilla 15-C, Concepción, Chile*
[6]*Instituto de Astronomía, Universidad Católica del Norte, Av. Angamos 0610, Antofagasta, Chile*
[7]*Space Telescope Science Institute, 3700 San Martin Drive, Baltimore, MD 21218, USA*
[8]*European Southern Observatory, Casilla 19001, Santiago, Chile*
[9]*Departamento de Física, Facultad de Ciencias Exactas, Universidad Andrés Bello, Av. Fernandez Concha 700, Las Condes, Santiago, Chile*
[10]*School of Physics and Astronomy, Sun Yat-sen University, Zhuhai 519082, People's Republic of China*

Accepted 2019 December 9. Received 2019 December 7; in original form 2019 May 11

ABSTRACT

In this article, we present a detailed chemical analysis of seven red giant members of NGC 6553 using high-resolution spectroscopy from VLT FLAMES. We obtained the stellar parameters ($T_{\rm eff}$, Log(g), $v_{\rm t}$, [Fe/H]) of these stars from the spectra, and we measured the chemical abundance for 20 elements, including light elements, iron-peak elements, α-elements, and neutron-capture elements. The metallicities in our sample stars are consistent with a homogeneous distribution. We found a mean of [Fe/H] $= -0.14 \pm 0.07$ dex, in agreement with other studies. Using the α-elements Mg, Si, Ca, and Ti, we obtain the mean of [α/Fe] $= 0.11 \pm 0.05$. We found a vertical relation between Na and O, characterized by a significant spread in Na and an almost non-existent spread in O. In fact, Na and Al are the only two light elements with a large intrinsic spread, which demonstrates the presence of multiple populations (MPs). An intrinsic spread in Mg is not detected in this study. The α, iron-peak, and neutron-capture elements show good agreement with the trend of the bulge field stars, indicating similar origin and evolution, in concordance with our previous studies for two other bulge globular clusters (NGC 6440 and NGC 6528).

Key words: stars: abundances – globular clusters: individual (NGC 6553) – Bulge.

1 INTRODUCTION

Having a complete picture of different components of our Galaxy will allow us to understand with more detail their formation, evolution, and the different astrophysical processes which have been involved during their lifetime. In fact, nowadays, our knowledge regarding the Milky Way has been greatly improved, thanks to a large number researchers and new surveys which use the latest generation of facilities such as the VLT FLAMES, VVV/VVVX survey (Minniti et al. 2010), the *Gaia*-ESO survey (Gilmore et al. 2012), SDSS-IV (Blanton et al. 2017), and the *Gaia* mission.

In this picture, undoubtedly the bulge of the Milky Way occupies an essential place. For this reason, there are more and more researchers studying distinct components or astrophysical processes in the bulge, such as dynamics (Beaulieu et al. 2000; Portail et al. 2017), chemistry (Grieco et al. 2012; Nandakumar et al. 2018), and even exoplanets (Sahu et al. 2006; Cortés, Minniti & Villanova 2019), among others. Since the bulge is likely the oldest component of our Galaxy, it can give us relevant information on its formation and subsequent evolution. One of the fundamental constituents of the bulge are globular clusters (GCs), less studied than their halo counterparts due to difficulties including high and often variable extinction, even across the small angular extent of a typical GC, as well as crowding and the difficulty in separating true bulge stars from intervening thin and thick disc stars.

Many studies have analysed in detail the GCs of our Galaxy, using high-, medium-, and low-resolution spectroscopy, and photometry in many different bands. However, most of these studies mainly focus on the more accessible sections of our Galaxy, avoiding in large part the bulge. These studies have uncovered an intrinsic intracluster variation in a variety of light elements, including C, N, O, Na, Mg, Al, and Si, which has become the major manifestation of the phenomenon known as multiple populations (MPs) in GCs.

★ E-mail: cesar.alejandro.munoz.g@gmail.com

MPs have been found in all galactic GCs, with only a few exceptions such as Ruprecht 106 (Villanova et al. 2013; Dotter et al. 2018). Moreover, most of these studies have focused on the detection of Na–O and Mg–Al anticorrelation (Carretta et al. 2009), which are related to several nucleosynthesis processes whose ejecta might then allow the formation of a new generation of stars in the GCs with a consequent spread in the relevant light element abundances.

Another exciting aspect is the spread in iron found in some galactic GCs (Johnson et al. 2008; Marino et al. 2011a, b; Da Costa et al. 2009; Carretta et al. 2010b; Origlia et al. 2011). However, this is still an open question that needs to be clarified, since in some GCs this spread is not clear, e.g. in the case of NGC 3201 (Muñoz, Geisler & Villanova 2013; Mucciarelli et al. 2015), or in other cases where iron spread has been found with more uncertain techniques. Indeed, Mauro et al. (2014) found indications of significant spreads in some bulge GCs using Calcium Triplet technique in combination with NIR photometry. We have investigated these claims in two previous studies (Muñoz et al. 2017, 2018), and here investigate a third cluster in this respect, NGC 6553.

In our initial papers on bulge GCs, we performed chemical tagging of NGC 6440 (Muñoz et al. 2017) and NGC 6528 (Muñoz et al. 2018). We found a very short extension in the Na–O anticorrelation, more consistent with a significant spread only in Na but not in O, and a chemical evolution somewhat different from their halo counterparts, but in agreement with the chemical evolution of the bulge of our Galaxy.

In an effort by our group to expand the study of the bulge GCs, we present in this article a detailed chemical analysis for the bulge GC NGC 6553. This is clearly a bulge GC, located at a distance of only 2.2 Kpc (2010 edition Harris 1996) from the Galactic Centre. Like most bulge GCs, it has a high nominal reddening of $E(B-V) = 0.63$ (2010 edition Harris 1996), with a complex differential reddening.

NGC 6553 has been the subject of several studies using a variety of techniques in different wavelengths. For example, Dias et al. (2016) studied this GC among other galactic GCs, using low-resolution spectroscopy. Tang et al. (2017) studied NGC 6553 using high-resolution spectroscopy from APOGEE (Majewski et al. 2017) part of the Sloan Digital Sky Survey III (Eisenstein et al. 2011). Also, Cohen et al. (2017) and Mauro et al. (2014) performed point spread function (PSF) photometry for a set of bulge GCs, which include NGC 6553, using data from the VVV survey (Minniti et al. 2010). Indeed, in this article, we take advantage of this photometry for use in target selection.

In the next section, we describe our observations and data reduction procedure, in Section 3, we describe in detail the method used to obtain the atmospheric parameters, errors, and chemical abundances. In Section 4, we present our results regarding iron-peak elements, alpha-elements, Na–O anticorrelation, Mg–Al–Na relations, and neutron capture elements. Finally, in Section 5, we summarize our main findings.

2 OBSERVATIONS AND DATA REDUCTION

We observed seven red giants stars in NGC 6553 with the fiber-fed multiobject FLAMES spectrograph mounted at the ESO VLT/UT2 telescope in Cerro Paranal (Chile) in period 93A (ESO program ID 093.D-0286, PI S. Villanova). The analyses of the stars observed with FLAMES were conducted using the blue and red arms of the high-resolution spectrograph UVES. We obtained a single spectra for each star with an exposure time of 2774 s.

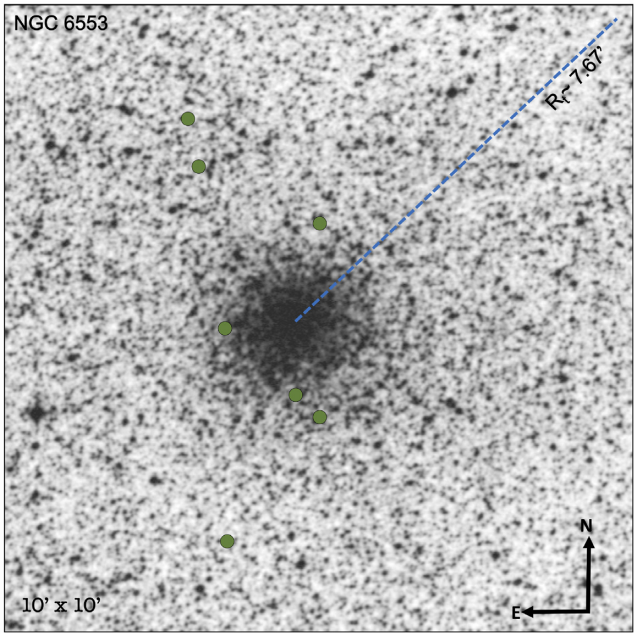

Figure 1. Distribution of the stars observed in NGC 6553 (green filled circles). The blue dashed line shows the extent of the tidal radius (2010 edition, Harris 1996).

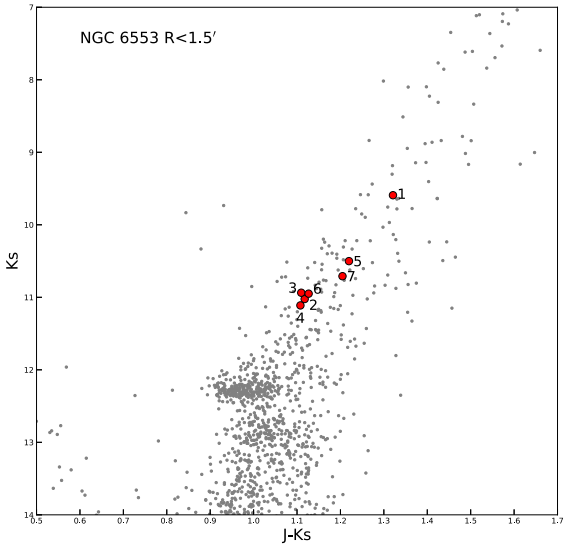

Figure 2. CMD of NGC 6553 from the VVV survey corrected by the VVV reddening maps (Gonzalez et al. 2012). The red filled circles represent our observed UVES sample.

The seven targets observed with FLAMES-UVES come from the membership list of NGC 6553 previously published in Saviane et al. (2012) and Mauro et al. (2014) using FORS2 Ca triplet spectroscopy and VVV photometry, whose spatial distribution is shown in Fig. 1. All the stars of our sample belong to the upper red giant branch (RGB), as can be seen in the colour–magnitude diagram (CMD) of the cluster (Fig. 2). FLAMES-UVES data have a spectral resolution of about $R \simeq 47\,000$. The data were taken with central wavelength 580 nm, which covers the wavelength range 476–684 nm. Our S/N is about 25 at 560 nm (lower chip) and about 30 at 650 nm (upper chip).

Table 1. Parameters of the observed stars for NGC 6553.

ID	RA (h:m:s)	Dec. (°:′:″)	J (mag)	H (mag)	K_s (mag)	RV_H (km s^{-1})	T_{eff} (K)	log(g)	[Fe/H] (dex)	v_t (km s^{-1})	Fe I/Fe II
1	18:09:15.66	−25:56:00.77	10.86	9.90	9.63	6.12 ± 0.21	4172 ± 15	1.21 ± 0.12	−0.17 ± 0.07	1.24 ± 0.04	85/10
2	18:09:15.71	−25:52:58.70	12.17	11.276	11.035	− 8.07 ± 0.19	3998 ± 16	1.19 ± 0.13	−0.06 ± 0.07	0.98 ± 0.07	82/9
3	18:09:17.51	−25:55:42.30	12.05	11.17	10.94	− 7.49 ± 0.41	4216 ± 19	1.34 ± 0.20	−0.19 ± 0.07	1.35 ± 0.05	92/10
4	18:09:22.39	−25:54:37.94	12.20	11.33	11.10	− 10.95 ± 0.27	4051 ± 16	1.06 ± 0.17	−0.07 ± 0.07	0.89 ± 0.10	88/11
5	18:09:22.43	−25:57:59.32	11.76	10.80	10.52	− 1.81 ± 0.42	4055 ± 22	1.40 ± 0.16	−0.16 ± 0.07	1.05 ± 0.12	101/13
6	18:09:23.98	−25:52:01.20	12.07	11.22	10.95	− 2.76 ± 0.26	4399 ± 16	1.94 ± 0.14	−0.08 ± 0.07	0.97 ± 0.10	92/11
7	18:09:24.67	−25:51:11.10	11.92	11.03	10.71	2.04 ± 0.31	4340 ± 20	1.74 ± 0.19	−0.22 ± 0.07	1.47 ± 0.06	81/8

Note. Column 12: numbers of line measured for Fe I and Fe II.

The reduction process includes bias and flat-field corrections, wavelength calibration, spectral rectification, and sky subtraction. We apply the same procedure described in our previous articles (Muñoz et al. 2017, 2018).

The mean radial velocity for NGC 6553 in our sample is -3.86 ± 2.12 km s^{-1}, the velocity dispersion is 5.62 km s^{-1}. This radial velocity is compatible with the values in the literature: Saviane et al. (2012) with four stars found a value of -9.0 ± 4.0 km s^{-1}, (2010 edition Harris 1996) quotes a value of -3.2 ± 1.5 km s^{-1}, and Tang et al. (2017) found a value of -0.14 ± 5.46 km s^{-1}.

Table 1 lists the stellar parameters of our sample: ID, the J2000 coordinates (RA and Dec.), J, H, K_s magnitudes from VVV PSF photometry, calibrated on the system of 2MASS (Mauro et al. 2014; Cohen et al. 2017), heliocentric radial velocity, T_{eff}, log(g), micro-turbulent velocity (v_t), and metallicity. Moreover, Table 2 shows the metallicity values from Saviane et al. (2012), Mauro et al. (2014), and Tang et al. (2017). The procedure for the determination of the atmospheric parameters is discussed in the next section.

3 ATMOSPHERIC PARAMETERS AND ABUNDANCES

We have analysed our sample of NGC 6553 stars using the local thermodynamic equilibrium (LTE) program MOOG (Sneden 1973). Atmospheric models were performed using ATLAS9 (Kurucz 1970) and the line list for the chemical analysis is the same described in Villanova & Geisler (2011) and widely used in several studies (Villanova et al. 2013; Muñoz et al. 2017, 2018; Mura-Guzmán et al. 2017; Rain et al. 2019). The stellar parameters T_{eff}, v_t, and log(g) were adjusted iteratively and new stellar models were calculated in an effort to remove trends in excitation potential and equivalent width versus abundance for T_{eff} and v_t, respectively, and to satisfy the ionization equilibrium for log(g). Fe I and Fe II were used for this latter objective. The [Fe/H] value of the model was changed at each iteration according to the output of the abundance analysis. Also, we present in Table 1 the uncertainties for T_{eff}, log g, and v_t, these were estimated following Gonzalez & Vanture (1998) and Neuforge-Verheecke & Magain (1997). The uncertainties for v_t were estimated using the standard deviation in the slope of the least-squares fit of abundance versus reduced equivalent width (EW), the uncertainties for T_{eff} were determined from the uncertainty of the least-squares fit of abundance versus excitation potential, in addition to the uncertainty in the slope due to the uncertainties in v_t. Finally to calculate the uncertainty in log g, we include the contribution from the uncertainty in T_{eff} in addition to the scatter in the Fe II line abundances.

In Fig. 3, we found good agreement among the stellar parameters derived in this study and from three different model isochrones with similar metallicity and with an age of 13 Gyr. The models used in this comparison are: PARSEC (Bressan et al. 2012), MESA (Dotter 2016; Choi et al. 2018), and the Dartmouth (Dotter et al. 2008) models. In Fig. 3, these models are plotted in green, blue, and black, respectively. Although, we note a small offset among the data and the isochrone, it is important take account that an offset of ∼100 K between photometric and spectroscopic T_{eff} can arise because of uncertainties in the mixing-length parameter and/or surface boundary condition (Choi et al. 2018). Also other studies find a similar mismatch especially associated with metal-rich stars (Ness et al. 2013).t

The reddening is high for most of the bulge GCs, and NGC 6553 is no exception. NGC 6553 has a colour excess of $E(B-V) = 0.63$ quoted by Harris (1996, 2010 edition) and Guarnieri et al. (1998) found a value of $E(B-V) = 0.70$. The potentially high differential reddening and high crowding make it difficult to obtain the stellar parameters. In order to avoid the effect of the extinction and the differential reddening in the measurement of the stellar parameters, we decided to calculate the stellar parameters directly from the spectra.

Table 2. Iron abundances from different authors for NGC 6553.

ID.	$[Fe/H]_{this\_work}$	$[Fe/H]_{S12}$[a]	[Fe/H][b]	[Fe/H][c]	[Fe/H][d]
1	−0.17 ± 0.07	− 0.44	− 0.27 ± 0.14	−0.15	–
2	−0.06 ± 0.07	0.10	− 0.02 ± 0.14	−0.13	−0.17
3	−0.19 ± 0.07	0.29	0.30 ± 0.14	−0.22	–
4	−0.07 ± 0.07	0.12	− 0.13 ± 0.14	−0.09	−0.16
5	−0.16 ± 0.07	0.24	0.12 ± 0.14	−0.13	–
6	−0.08 ± 0.07	− 0.06	0.09 ± 0.14	−0.10	−0.08
7	−0.22 ± 0.07	0.00	0.04 ± 0.14	−0.14	–

[a]Saviane et al. (2012).
[b]M14: Mauro et al. (2014).
[c]Dias et al. (2016).
[d]Tang et al. (2017).

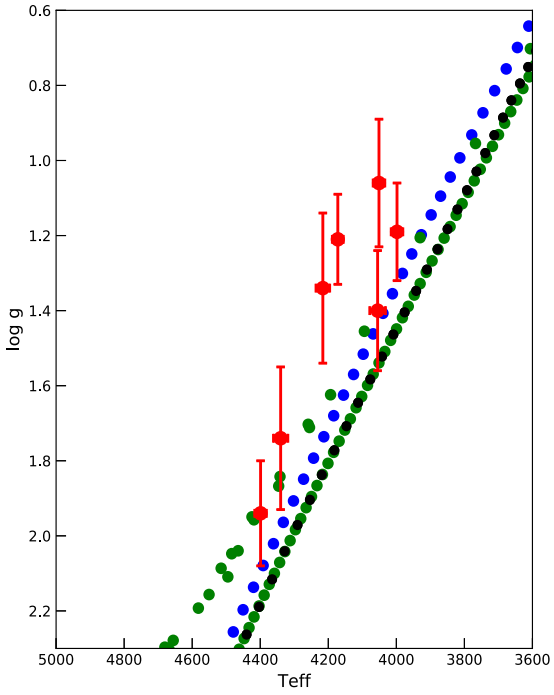

Figure 3. Log (g) versus $T_{\rm eff}$ for NGC 6553. The black points display an isochrone with a metallicity of −0.16 dex, [α/Fe] = +0.20 dex and age of 13 Gyr (Dartmouth isochrone, Dotter et al. 2008). The green points is an isochrone with a metallicity of −0.16 dex and age of 13 Gyr (PARSEC isochrone, Bressan et al. 2012). The blue point is an isochrone with a metallicity of −0.16 dex and age of 13 Gyr (MESA isochrone, Choi et al. 2016; Dotter 2016).

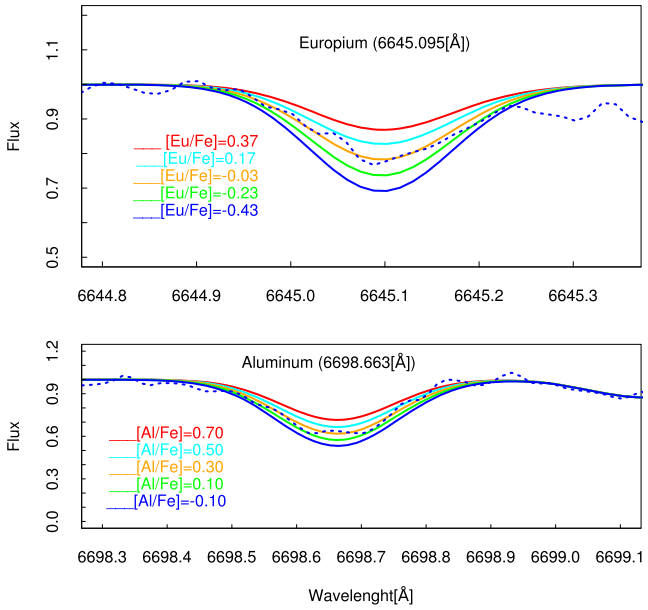

Figure 4. Spectrum synthesis fits for europium (upper panel) and aluminium (lower panel) lines for the star #5 and #4, respectively. The dashed line is the observed spectrum, and the solid colour lines show the synthesized spectra corresponding to different abundances.

We used EWs of the spectral lines and the spectrum-synthesis method to obtain abundances of a large number of elements, which are listed in Table 3. We used the spectrum-synthesis method for lines affected by blending. In this case, we generated five synthetic spectra with different abundances for each line, and we estimated the best-fitting value as the one that minimizes the rms scatter. Fig. 4 shows an example of this method for two different lines. We carefully excluded the telluric contaminated lines in our analysis. The adopted solar abundances we use are reported in Table 3.

We carry out an internal error analysis varying the stellar parameters ($T_{\rm eff}$, log(g), [Fe/H], and $v_{\rm t}$) and redetermining abundances of star #1, which is representative of our whole sample (see Table 4). Parameters were varied by $\Delta T_{\rm eff}$ = +50 K, Δlog(g) = +0.13, Δ[Fe/H] = +0.03 dex, and $\Delta v_{\rm t}$ = +0.09 km s^{-1}, which we estimated as our typical internal errors. The quantity of variation of the parameter was calculated through three stars representative of our sample (#1, #2, and #7) with relatively low-, intermediate-, and high-effective temperature, respectively, according to the method that was performed by Marino et al. (2008). The error introduced by the uncertainty on the EW ($\sigma_{\rm S/N}$) was calculated by dividing the rms scatter by the square root of the number of the lines used for a given element and a given star. For elements whose abundance was obtained by spectrum synthesis, the error is given in the output of the fitting procedure. The error for each [X/Fe] ratio as a result of uncertainties in atmospheric parameters and $\sigma_{\rm S/N}$ are showed in Table 4. The total internal error ($\sigma_{\rm tot}$) is given by

$$\sigma_{\rm tot} = \sqrt{\sigma^2_{T_{\rm eff}} + \sigma^2_{\rm log(g)} + \sigma^2_{v_{\rm t}} + \sigma^2_{\rm [Fe/H]} + \sigma^2_{\rm S/N}}. \quad (1)$$

In Table 4, we compare the total internal error for all the elements measured with the observed error (standard deviation of the sample).

4 RESULTS

In this section, we will discuss and examine in detail our results. Furthermore, we compare them with the literature, focusing on our previous articles (Muñoz et al. 2017, 2018), which present an identical analysis of two bulge GCs (NGC 6440 and NGC 6528).

4.1 Iron

We found a mean [Fe/H] value for the cluster of [Fe/H] = −0.14 ± 0.07 dex. The scatter observed in this cluster is $\sigma_{\rm obs}$ = 0.06, which is consistent with the total expected observational error of $\sigma_{\rm tot}$ = 0.07, indicating a homogeneous iron content. Saviane et al. (2012) using Ca II triplet found a mean in iron of [Fe/H] = −0.16 ± 0.06 in their sample. We present in Table 2 the targets which we have in common. Mauro et al. (2014) found a mean value in iron of [Fe/H] = 0.02 using the Ca II triplet equivalent widths from Saviane et al. (2012) but using near-IR instead of optical photometry for the analysis (see Table 2). These studies are compatible with our results taking into account the uncertainties. It is interesting to note that Saviane et al. (2012) found a scatter of σ = 0.06, compatible with no spread in iron in agreement with our finding of homogeneity in iron. Mauro et al. (2014) found a larger scatter of σ = 0.17. However, this value is similar to their errors, indicating homogeneity in metallicity, in agreement with our results.

Tang et al. (2017) using high-resolution spectra in a sample of 10 members of NGC 6553 from APOGEE found a mean of [Fe/H] = −0.15 ± 0.05 with a spread in iron of σ = 0.05, in excellent agreement with our sample. We have three stars in common with Tang (Table 2) – their results for these stars are compatible with our results taking into account the errors.

Table 3. Abundances of the observed stars for NGC 6553.

El.	1	2	3	4	5	6	7	Cluster[a]	Sun
[O/Fe]	− 0.17	− 0.14	− 0.05	− 0.16	− 0.06	0.06	0.03	− 0.07 ± 0.03	8.83
	±0.03	±0.03	±0.05	±0.04	±0.05	±0.05	±0.04		
$[Na/Fe]_{NLTE}$	0.24	− 0.09	0.47	0.22	0.60	− 0.00	0.18	+0.23 ± 0.09	6.32
	±0.03	±0.05	±0.06	±0.05	±0.06	±0.06	±0.05		
[Mg/Fe]	0.27	0.23	0.22	0.17	0.07	0.14	0.29	+0.20 ± 0.03	7.56
	±0.04	±0.05	±0.04	±0.06	±0.05	±0.04	±0.05		
[Al/Fe]	0.28	0.13	0.34	0.34	0.53	0.21	0.40	+0.32 ± 0.05	6.43
	±0.03	±0.04	±0.04	±0.04	±0.04	±0.04	±0.04		
[Si/Fe]	0.06	0.06	0.22	− 0.29	− 0.36	− 0.31	0.21	− 0.06 ± 0.09	7.61
	±0.03	±0.05	±0.06	±0.05	±0.06	±0.05	±0.06		
[Ca/Fe]	− 0.06	− 0.15	− 0.05	− 0.04	0.15	0.04	− 0.04	− 0.02 ± 0.03	6.39
	±0.05	±0.06	±0.07	±0.07	±0.06	±0.07	±0.08		
[Sc/Fe]	− 0.01	0.02	− 0.16	− 0.26	− 0.09	− 0.34	0.17	+0.09 ± 0.06	3.12
	±0.03	±0.05	±0.06	±0.05	±0.06	±0.05	±0.06		
[Ti/Fe]	0.17	0.20	0.24	0.31	0.56	0.43	0.31	+0.32 ± 0.05	4.94
	±0.06	±0.05	±0.06	±0.05	±0.07	±0.06	±0.06		
[V/Fe]	0.33	0.43	0.36	0.48	0.85	0.58	0.38	+0.48 ± 0.07	4.00
	±0.07	±0.05	±0.05	±0.07	±0.06	±0.07	±0.05		
[Cr/Fe]	0.02	− 0.10	− 0.09	− 0.03	0.18	− 0.02	0.03	0.00 ± 0.03	5.63
	±0.09	±0.06	±0.09	±0.10	±0.09	±0.09	±0.05		
[Mn/Fe]	− 0.09	− 0.10	0.10	− 0.27	− 0.06	− 0.37	− 0.22	− 0.14 ± 0.06	5.37
	±0.05	±0.07	±0.06	±0.07	±0.06	±0.06	±0.07		
[Fe/H]	− 0.17	− 0.06	− 0.19	− 0.07	− 0.16	− 0.08	− 0.22	− 0.14 ± 0.02	7.50
	±0.02	±0.03	±0.02	±0.02	±0.03	±0.03	±0.02		
[Ni/Fe]	0.22	0.23	0.21	0.36	0.38	0.21	0.18	+0.26 ± 0.03	6.26
	±0.06	±0.06	±0.07	±0.08	±0.07	±0.08	±0.08		
[Cu/Fe]	0.32	0.40	0.12	0.28	0.28	− 0.17	0.41	+0.23 ± 0.08	4.19
	±0.07	±0.06	±0.08	±0.08	±0.09	±0.08	±0.08		
[Y/Fe]	0.03	0.07	0.26	0.37	0.86	0.17	− 0.03	+0.25 ± 0.11	2.25
	±0.06	±0.06	±0.07	±0.07	±0.06	±0.07	±0.06		
[Zr/Fe]	− 0.52	0.03	− 0.45	− 0.34	0.22	− 0.70	− 0.50	− 0.32 ± 0.16	2.56
	±0.04	±0.05	±0.04	±0.08	±0.05	±0.05	±0.06		
[Ba/Fe]	− 0.01	0.29	− 0.01	0.13	0.10	− 0.40	0.18	+0.04 ± 0.08	2.34
	±0.05	±0.05	±0.06	±0.07	±0.06	±0.07	±0.05		
[Ce/Fe]	− 0.24	− 0.07	− 0.10	− 0.12	0.03	− 0.31	− 0.08	− 0.13 ± 0.04	1.53
	±0.08	±0.04	±0.04	±0.09	±0.08	±0.08	±0.10		
[Nd/Fe]	− 0.29	− 0.01	− 0.38	− 0.41	− 0.19	− 0.76	− 0.37	− 0.34 ± 0.09	1.59
	±0.06	±0.08	±0.06	±0.07	±0.10	±0.08	±0.07		
[Eu/Fe]	− 0.06	0.06	0.08	− 0.03	− 0.01	− 0.23	0.02	− 0.02 ± 0.04	0.52
	±0.04	±0.03	±0.04	±0.05	±0.04	±0.04	±0.05		

Notes. Columns 2–8: abundances of the observed stars. Column 9: mean abundance for the cluster. Column 10: abundances adopted for the Sun in this paper. Abundances for the Sun are indicated as log ϵ (El.). The errors presented for each abundance were calculated by dividing the rms scatter by the square root of the number of the lines used for a given element and a given star. For elements whose abundance were obtained by spectrum synthesis, the error is the output of the fitting procedure.
[a]The errors are the statistical errors obtained of the mean.

Dias et al. (2016) studied the low-resolution optical spectra of the same stars from Saviane et al. (2012). They used a full-spectrum fitting technique to derive the abundance. They found an average metallicity for NGC 6553 of [Fe/H] = −0.13 ± 0.01 in agree with our finding. Also, we found good accordance star by star (see Table 2).

Finally, Ernandes et al. (2018) study the iron-peak elements in four stars member of NGC 6553 using high-resolution spectroscopy. They found a metallicity of [Fe/H] = −0.20 dex with a scatter of σ = 0.02, in good agreement again with our results.

4.2 Iron-peak elements

We have measured the abundance of seven iron-peak elements: Sc, V, Cr, Mn, Fe, Ni, and Cu (see Table 3 and Fig. 5). We have analysed the iron in detail in the previous section.

In Fig. 5, we plotted iron-peak elements versus [Fe/H] comparing with our previous studies for NGC 6440 (Muñoz et al. 2017) and NGC 6528 (Muñoz et al. 2018). We found good agreement with NGC 6528 for the case of Cr, Ni, and Cu. All of these elements are supersolar except for Mn. Vanadium shows a very high supersolar abundance; however, the observational error is quite large for this element.

Three of the iron-peak elements (Cr, Mn, Ni) were analysed in APOGEE DR13. The mean values of the 10 stars presented in Tang et al. (2017) are: [Cr/Fe] = 0.00, [Mn/Fe] = 0.04, [Ni/Fe] = 0.06. Cr shows the same mean value found in this study as in Tang et al. (2017). V and Cu given by APOGEE DR13 are subject to large uncertainties (Tang et al. 2017), therefore, we made no comparison for V and Cu.

Table 4. Estimated errors on abundances for NGC 6553, due to errors on atmospherics parameters and to spectral noise, compared with the observed errors.

ID	$\Delta T_{\rm eff} = 50$ K	$\Delta\log(g) = 0.13$	$\Delta v_{\rm t} = 0.09$	Δ[Fe/H] = 0.03	$\sigma_{\rm S/N}$	$\sigma_{\rm tot}$	$\sigma_{\rm obs}$
Δ([O/Fe])	0.01	− 0.02	0.06	0.02	0.03	0.07	0.09
Δ([Na/Fe])	− 0.08	− 0.04	0.00	− 0.06	0.03	0.11	0.24
Δ([Mg/Fe])	− 0.07	0.00	0.03	0.01	0.04	0.09	0.08
Δ([Al/Fe])	− 0.01	0.01	0.05	0.03	0.03	0.07	0.13
Δ([Si/Fe])	0.07	− 0.07	− 0.08	0.06	0.05	0.15	0.25
Δ([Ca/Fe])	− 0.07	− 0.01	0.03	− 0.02	0.05	0.09	0.09
Δ([Sc/Fe])	0.04	− 0.04	− 0.01	0.00	0.03	0.06	0.17
Δ([Ti/Fe])	− 0.06	0.00	− 0.08	− 0.01	0.06	0.11	0.14
Δ([V/Fe])	− 0.06	0.00	− 0.10	− 0.01	0.07	0.14	0.18
Δ([Cr/Fe])	− 0.09	− 0.05	− 0.01	− 0.04	0.09	0.15	0.09
Δ([Mn/Fe])	0.10	0.12	0.10	0.04	0.05	0.19	0.16
Δ([Fe/H])	0.01	0.02	− 0.06	0.00	0.02	0.07	0.06
Δ([Ni/Fe])	0.12	0.11	0.15	0.13	0.06	0.26	0.08
Δ([Cu/Fe])	0.06	0.10	0.09	0.12	0.07	0.20	0.20
Δ([Y/Fe])	0.12	0.13	0.16	0.16	0.06	0.29	0.30
Δ([Zr/Fe])	0.05	0.06	0.11	0.07	0.04	0.16	0.33
Δ([Ba/Fe])	0.1	0.07	0.15	0.11	0.05	0.23	0.22
Δ([Ce/Fe])	0.13	0.08	0.13	0.10	0.08	0.24	0.11
Δ([Nd/Fe])	0.06	0.05	0.10	0.08	0.06	0.15	0.23
Δ([Eu/Fe])	− 0.01	0.01	0.09	− 0.03	0.04	0.10	0.10

Ernandes et al. (2018) studied some iron-peak elements (Sc, V, Mn, Cu, and Zn) in NGC 6553. Their results are compatible with our results for Sc and Cu, taking into account the uncertainties. The more substantial difference is for Vanadium, although our error for this element is large.

Similar to the case of NGC 6528 and NGC 6440, the super solar abundance for most of the iron-peak elements is evidence of early pollution by SN explosion(s).

4.3 α-elements

α-elements are suggested to come from SN II explosions at an early epoch. We managed to measure five α elements (O, Mg, Si, Ca, and Ti). NGC 6553 shows very similar behaviour to NGC 6528 for the case of the α-elements, with a very strong overabundance relative to the solar scale for Mg and Ti and with solar abundance for O, Si, and Ca.

Using the α-elements Mg, Si, Ca, and Ti to obtain the mean, we obtain [α/Fe] $= 0.11 \pm 0.05$.

All the bulge GCs of our studies (NGC 6440, NGC 6528, and NGC 6553), and including NGC 6441 (Gratton et al. 2006, 2007) and HP-1 (Barbuy et al. 2016), show good agreement with the trend of the bulge (see Figs 6 and 7) for the alpha elements in general. Although, in the case of NGC 6553, this one shows some compatibility with the bulge trend as well with the disc trend (see Fig. 7).

We did not find a clear Si spread in NGC 6553 ($\sigma_{\rm tot} = 0.15$, $\sigma_{\rm obs} = 0.25$), similar to the case of Tang et al. (2018). It is interesting to note that in NGC 6528 (Muñoz et al. 2018), we found a similar behaviour ($\sigma_{\rm tot} = 0.11$, $\sigma_{\rm obs} = 0.14$). An intrinsic spread in silicon is mainly found in metal-poor GCs or massive GCs (Ventura et al. 2012; D'Antona et al. 2016; Tang et al. 2018). Therefore, we did not expect to find a spread in silicon in NGC 6553 or NGC 6528. However, the elements for which we did expect to find a significant spread, viz. O and Mg or both, in fact show little or no scatter, basically equal to the total error (Table 4). We will discuss O and Mg in the next sections.

4.4 Na–O anticorrelation

Without a doubt, the Na–O anticorrelation has given us a powerful tool to study the MPs in GCs. Currently, virtually all old massive GCs clearly show this remarkable anticorrelation with at least one clear exception – Ruprecht 106 (Villanova et al. 2013; Dotter et al. 2018). However, it has been established that the extension of this anticorrelation is mainly connected with the mass and metallicity of the GC (Carretta et al. 2009, 2010b, 2011, 2015).

In our previous articles (Muñoz et al. 2017, 2018), we have found in NGC 6528 and NGC 6440 a peculiar O–Na anticorrelation, basically vertical and with a very short, if any, horizontal extension, implying a Na but no significant O spread. NGC 6553 follows this pattern, with a very low scatter in O of $\sigma_{\rm obs} = 0.09$ (compared to a total expected error of 0.07) and a more significant spread in Na of $\sigma_{\rm obs} = 0.24$ (compared to an expected error of 0.11). A similar pattern was shown in Tang et al. (2017): a small scatter in oxygen ($\sigma_{\rm obs} = 0.05$), and a spread much greater in Na ($\sigma_{\rm obs} = 0.15$) in comparison with their expected error. Their scatter values are very close to our results (see Fig. 8).

Our results are in agreement with the mentioned in various articles about the extension of the anticorrelation Na–O and its dependence on cluster mass (Carretta et al. 2009, 2010b, 2011, 2015). The GCs from our previous studies (i.e. NGC 6440 and NGC 6528) including the one presented here – NGC 6553, have masses between $(2.35 \pm 0.19) \times 10^5$ and $(8.96 \pm 1.85) \times 10^5$ $M_\odot$ (Baumgardt & Hilker 2018). Basically, these are intermediate mass GCs in comparison with other Galactic GCs. We find definite evidence that such intermediate mass bulge GCs have at most a short, almost vertical Na–O anticorrelation, extension, without a significant spread in oxygen. On the other hand, contrasting its results with NGC 6441 (Gratton et al. 2006, 2007), a massive bulge GCs of $(1.23 \pm 0.01) \times 10^6$ $M_\odot$ (Baumgardt & Hilker 2018), we noticed a broader extension of the correlation. Finally, comparing with the GC HP 1 with a low mass of $(1.11 \pm 0.38) \times 10^5$ $M_\odot$(Baumgardt & Hilker 2018), which have an unclear O–Na anticorrelation (Barbuy et al. 2016), although HP 1 is the most metal poor among the GCs compared in this research, with a metallicity

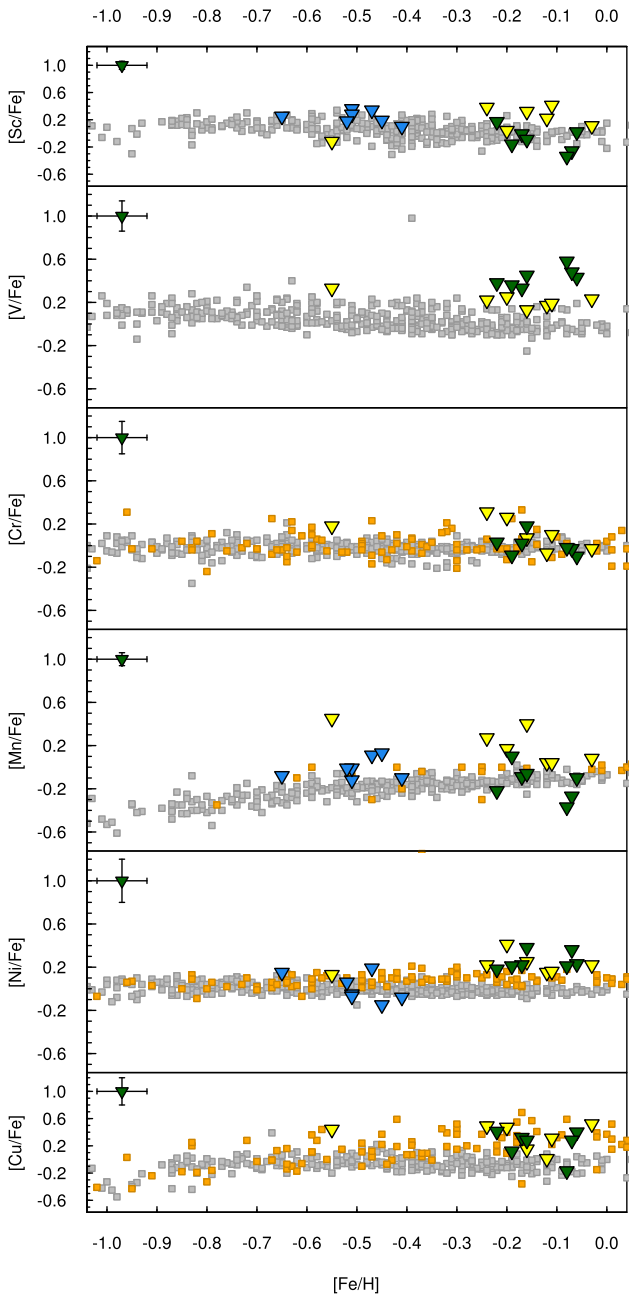

Figure 5. [Sc, V, Cr, Mn, Ni, Cu/Fe] versus [Fe/H]. Filled dark green triangles are our data for NGC 6553 (this study), Filled yellow triangles are our data for NGC 6528 (Muñoz et al. 2018), filled blue triangles: NGC 6440 (Muñoz et al. 2017), filled orange squares: bulge field stars (Barbuy et al. 2013; Johnson et al. 2014), and filled grey squares: halo and disc stars (Fulbright 2000; Reddy et al. 2003; Reddy, Lambert & Allende Prieto 2006; François et al. 2007).

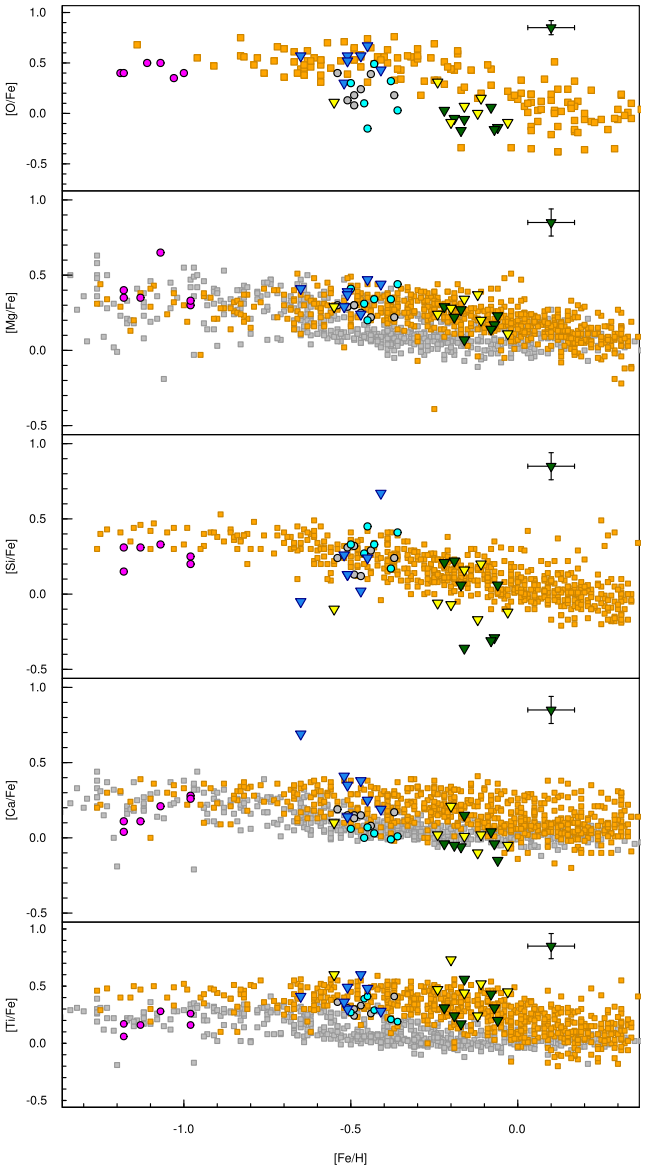

Figure 6. [O/Fe], [Mg/Fe], [Si/Fe], [Ca/Fe], [Ti/Fe] versus [Fe/H]. Filled dark green triangles are our data for NGC 6553 (this study), filled yellow triangles are our data for NGC 6528 (Muñoz et al. 2018), filled blue triangles: NGC 6440 (Muñoz et al. 2017), filled cyan circles: NGC 6441 (Gratton et al. 2006, 2007), filled grey circles: NGC 5927 (Mura-Guzmán et al. 2017), filled magenta triangles: HP1 (Barbuy et al. 2016), filled orange squares: bulge field stars (Gonzalez et al. 2012), and filled grey squares: halo and disc fields stars (Venn et al. 2004).

of [Fe/H] $= -1.06 \pm 0.10$ dex (Barbuy et al. 2016). Therefore, apparently there is a relationship between the mass and metallicity of the bulge GCs with their Na–O extension, in agreement with the literature.

4.5 Mg–Al and Na–Al

The study of the relationship between Mg and Al is another useful tool when studying MPs in GCs. Many authors have found an anticorrelation between these two elements (Carretta et al. 2009; Mészáros et al. 2015), but unlike the Na–O anticorrelation, this is present in fewer GCs studied so far. Nevertheless, similar to the case of Na–O, the extension of this anticorrelation strongly depends on mass and metallicity (Pancino et al. 2017).

Similar to the case of NGC 6528 from our previous study, we have not found an Mg–Al anticorrelation in this cluster (see Fig. 9). The spread of Mg is basically the same as the total error ($\sigma_{\rm tot} = 0.09$; $\sigma_{\rm obs} = 0.08$) and the spread of Al is somewhat greater than the total error ($\sigma_{\rm tot} = 0.07$; $\sigma_{\rm obs} = 0.13$). These results are in agreement with the result presented by Tang et al. (2017). They found a mean of Mg

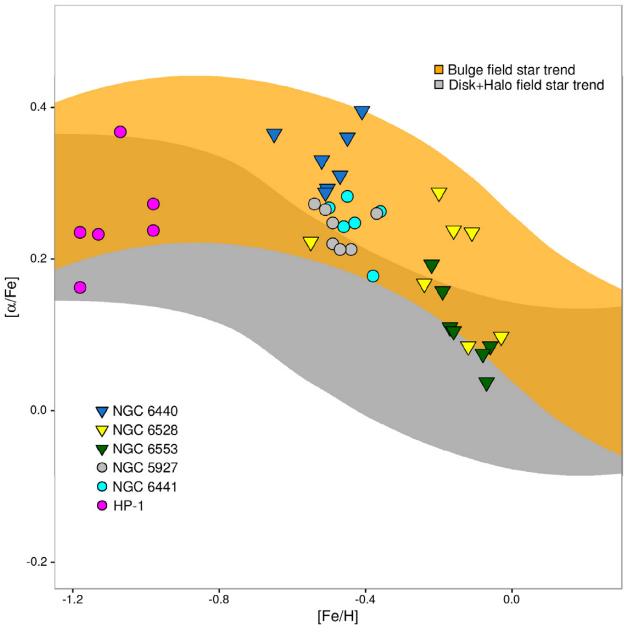

Figure 7. [α/Fe] versus [Fe/H]. Filled dark green triangles are our data for NGC 6553 (this study). Filled yellow triangles: NGC 6528, filled blue triangles: NGC 6440 (Muñoz et al. 2017), filled cyan circles: NGC 6441 (Gratton et al. 2006, 2007), filled grey circles: NGC 5927(Mura-Guzmán et al. 2017), filled magenta triangles: HP1 (Barbuy et al. 2016), filled orange squares: bulge field stars(Gonzalez et al. 2012), filled grey squares: halo and disc fields stars (Venn et al. 2004).

of [Mg/Al] = 0.15 with a scatter of $\sigma = 0.02$, while in the case of Al they found a mean of [Al/Fe] = 0.20 with a scatter of (σ = 0.14).

We build a plot using Na and Al (see Fig. 9), the light elements showing the most significant spread in our sample. We found a good agreement with bulge field star trend with an important extension. The spread in these elements allows us to verify the presence of MPs in this GC. Also, again we found a good concordance with the bulge GC NGC 6528. Finally, there are regions in this diagram where it is possible to disentangle bulge and disc stars regardless if they are in clusters or the field (see Fig. 9).

4.6 Neutron-capture elements

We measured the abundances for five neutron-capture elements: Zr, Ba, Ce, Nd, and Eu.

As seen in Fig. 10, these elements show a gradual decrease with increasing metallicity. This effect is due to the enrichment of iron from SN Ia (Van der Swaelmen et al. 2016).

The five elements show good agreement with the bulge field star trend, basically solar abundance for the case of Ba and Eu, and subsolar for the case of Nd and Zr with a value around −0.3 dex (see Fig. 10).

Comparing our results from NGC 6553 with NGC 6528 (Muñoz et al. 2018), we observe a good agreement for Zr and Ba. But, we find a significant difference in Eu of 0.23 dex.

The ratio of [Ba/Eu] shown in Fig. 11 is a good indicator of the contribution of the s-process versus r-process during the evolution of our Galaxy. In this plot we notice an increase of the [Ba/Eu] versus [Fe/H] for the bulge field stars, suggesting some contribution from the AGB stars around the solar metallicity (Van der Swaelmen et al. 2016).

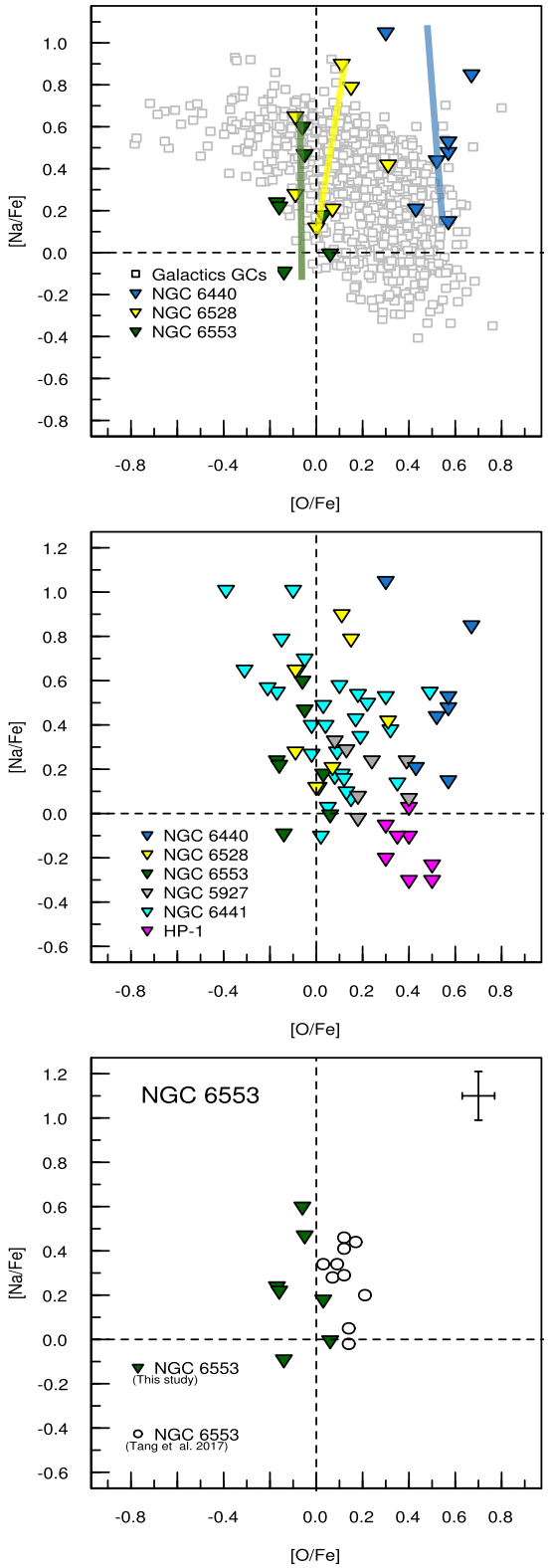

Figure 8. [O/Fe] versus [Na/Fe]. Filled dark green triangles are our data for NGC 6553, filled yellow triangles: NGC 6528 (Muñoz et al. 2018), filled blue triangles: NGC 6440 (Muñoz et al. 2017), filled grey triangles: NGC 5927 (Mura-Guzmán et al. 2017), filled cyan triangles: NGC 6441 (Gratton et al. 2006, 2007), filled magenta triangles: HP1 (Barbuy et al. 2016), filled grey square: Galactic GCs from Carretta et al. (2009), and open circles: NGC 6553 (Tang et al. 2017). The solid vertical line represents the trend in each GC.

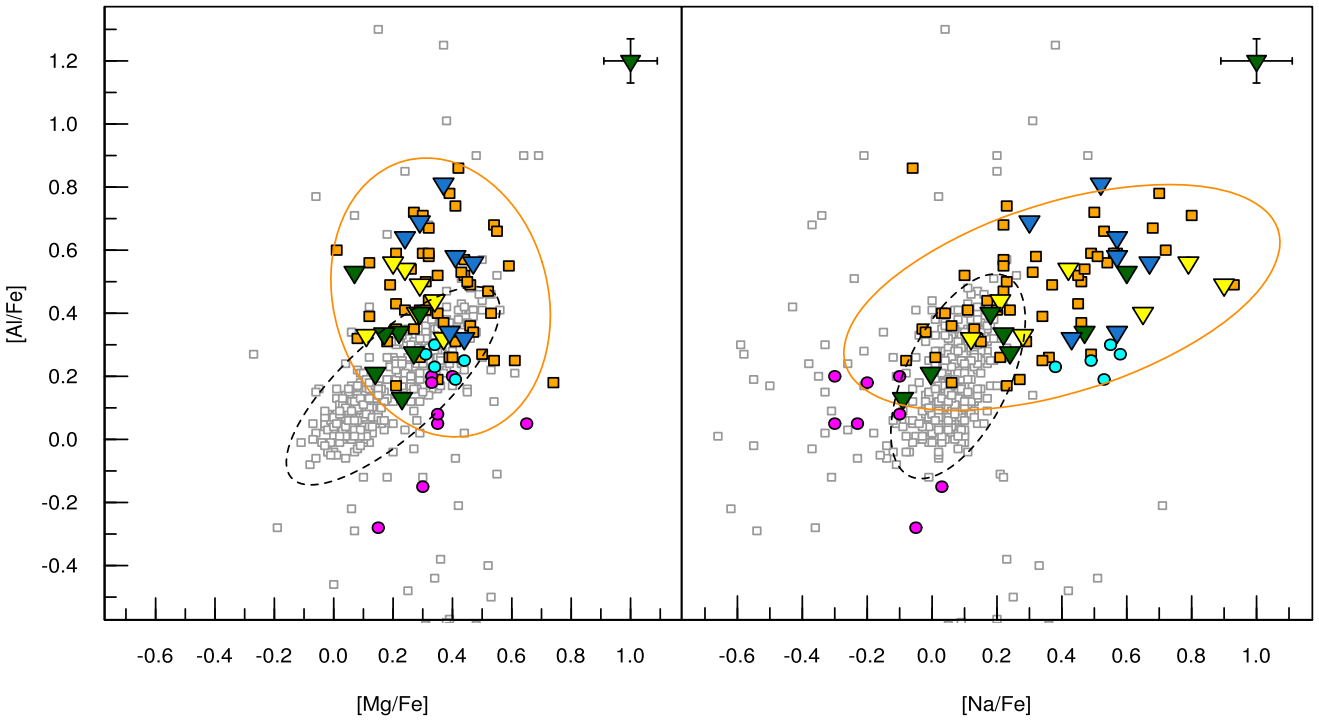

Figure 9. [Mg/Fe] versus [Al/Fe] and [Na/Fe] versus [Al/Fe]. Filled dark green triangles are our data for NGC 6553, filled yellow triangles: NGC 6528 (Muñoz et al. 2018), filled blue triangles: NGC 6440 (Muñoz et al. 2017), filled cyan triangles: NGC 6441 (Gratton et al. 2006, 2007), filled magenta triangles: HP1 (Barbuy et al. 2016), filled orange squares: bulge field stars (Lecureur et al. 2007), and filled grey squares: halo and disc fields stars (Fulbright 2000; Reddy et al. 2003; Cayrel et al. 2004; Barklem et al. 2005; Reddy et al. 2006).

We noticed that the results for our studies with NGC 6440 (Muñoz et al. 2017), NGC 6528 (Muñoz et al. 2018), and NGC 6553 (this study) are compatible with the bulge field stars trend. Specifically, regarding NGC 6553, we note a nucleosynthetic history dominated by s-process, indicating an area of formation mainly enriched by AGB stars at the early epoch (Van der Swaelmen et al. 2016).

5 CONCLUSIONS

In this article, we have derived detailed chemical abundances for the GC NGC 6553 from seven RGB star members. Using FLAMES-UVES data, we measured the chemical abundances of 20 elements, together with an accurate measurement of the errors. We have performed a detailed comparison with other bulge GCs studied homogeneously as part of our previous studies (Muñoz et al. 2017, 2018) and also compared to results in the literature for other bulge GCs (NGC 6441 and HP 1), as well as for field stars from the halo, disc, and the bulge.

Summarizing the most import results, NGC 6553 is one of the most metal-rich among Galactic GCs; the mean in metallicity found in our sample is [Fe/H] $= -0.14 \pm 0.07$ dex, and is homogeneous in iron content.

Using the α-elements Mg, Si, Ca, and Ti, we obtain the mean of [α/Fe] $= 0.11 \pm 0.05$. Overall, the α-elements, iron-peak elements and heavy elements measured for NGC 6553, show a good agreement with the bulge field stars trend as we can see in Figs 5, 7, 6, and 10. Although, it is possible to observe in this GC some compatibility with the disc trend (see Fig. 7), in agreement with the finding by Zoccali et al. (2001). However, we found very good accordance with NGC 6528, another bulge GCs, and with the general chemical patterns of the bulge.

Our most important finding is of a vertical Na–O relation, with a significant intrinsic spread in Na, but almost non-existent in the case of oxygen. This is compatible with the other bulge GCs NGC 6528 and NGC 6440 from our previous studies (Muñoz et al. 2017, 2018). This short extension in the Na–O anticorrelation found in these clusters (NGC 6553, NGC 6528, and NGC 6440) is in agreement with that found by Carretta in his previous studies (Carretta et al. 2010a, 2011, 2015) regarding the mass of the GCs. None the less, Carretta mentions other factors that may play a role in this regard. Metallicity is another important factor, considering that these three GCs are metal-rich among galactic GCs, with a metallicity between [Fe/H] $= -0.50$ to -0.14 dex, this would be in agreement with what was mentioned by Carretta et al. (2009) and Gratton et al. (2010, 2011) about the extension of the Na–O and the metallicity. Other factors must come into play, such as the environment of formation and evolution of these GCs, taking into account that these three metal-rich GCs are members of the bulge of our Galaxy. It is also important to note that our samples are small, only seven stars in each bulge GCs, therefore we need to increase it to be conclusive about our finding.

Likewise, we have found no Mg–Al anticorrelation, similar to the case of NGC 6528 (Tang et al. 2017). Finally, we detect the presence of MPs in this bulge GCs mainly via the spread in Na and Al (see Fig. 9).

We measured five neutron capture elements, which follow the trend of the bulge field stars and the bulge GCs from our previous studies (NGC 6440 and NGC 6528). [Ba/Eu] versus [Fe/H] is dominated by s-process material, indicating a formation mainly enriched by AGB stars at an early epoch.

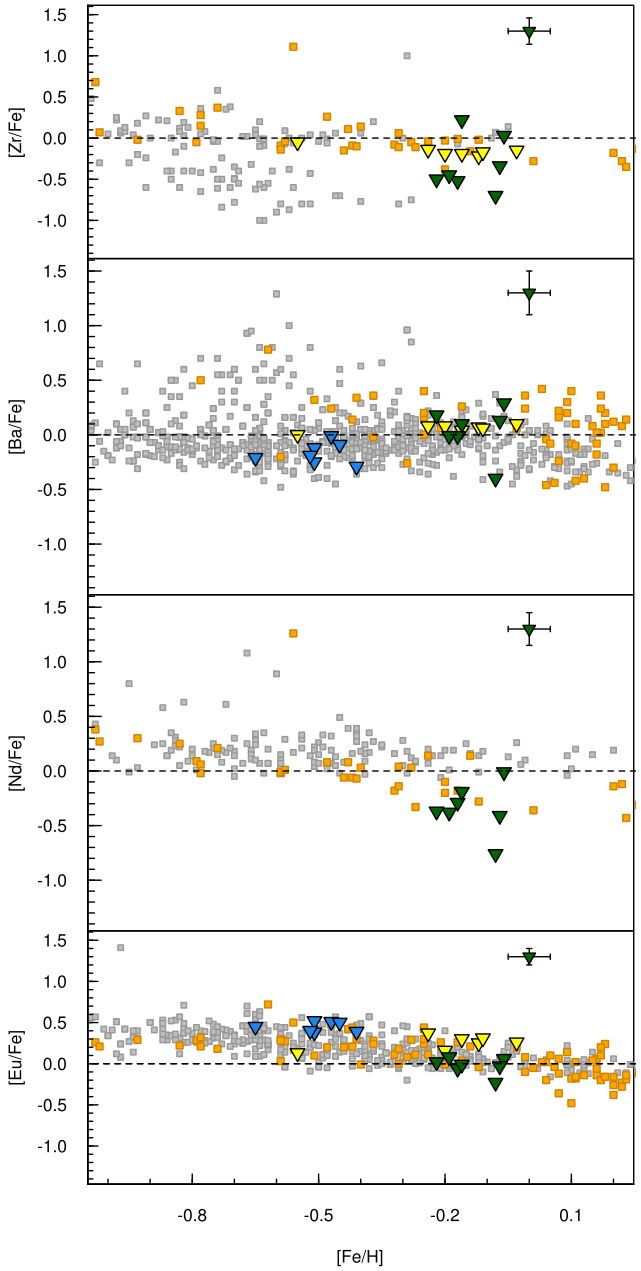

Figure 10. [Eu, Ba/Fe] versus [Fe/H]. Filled dark green triangles are our data for NGC 6553, filled yellow triangles: NGC 6528 (Muñoz et al. 2018), filled blue triangles: NGC 6440 (Muñoz et al. 2017), filled orange squares: bulge field stars (Van der Swaelmen et al. 2016), and filled grey squares: halo and disc stars (Fulbright 2000; Venn et al. 2004; Barklem et al. 2005; Reddy et al. 2006; François et al. 2007).

Finally, we have presented in this research a new chemical tagging for the GC NGC 6553. Together with the other two bulge GCs we have studied, these provide a homogeneous data set for more than a single bulge GC. Clearly the bulge deserves much more dedicated studies to uncover the many hidden secrets it must contain about the nature of the formation and evolution of this primary Galactic component. Such a study recently begun is the CAPOS (bulge Cluster APOgee Survey) project designed to observe the bulk of the bulge GCs using the high resolution, near-IR multiplexing capabilities of the APOGEE spectrograph.

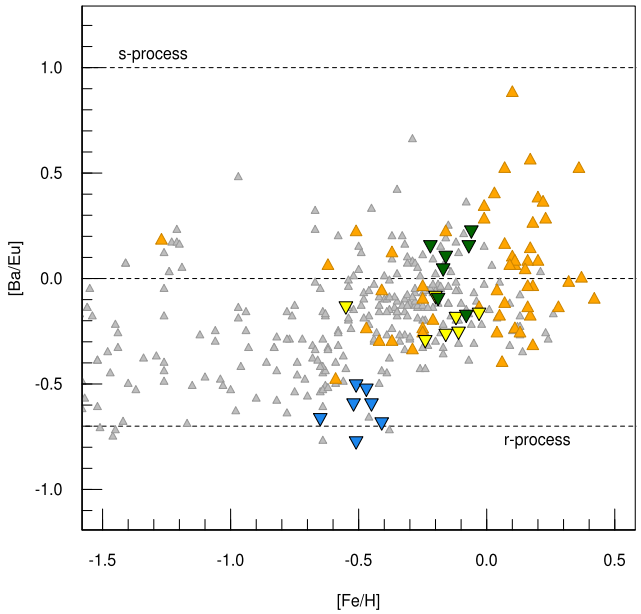

Figure 11. [Ba/Eu] versus [Fe/H]. Filled dark green triangles are our data for NGC 6553, filled yellow triangles: NGC 6528 (Muñoz et al. 2018), filled blue triangles: NGC 6440 (Muñoz et al. 2017), filled orange squares: bulge field stars (Van der Swaelmen et al. 2016), and filled grey squares: halo and disc stars (Fulbright 2000; Venn et al. 2004; Barklem et al. 2005; Reddy et al. 2006; François et al. 2007).

ACKNOWLEDGEMENTS

This work is Based on observations collected at the European Organisation for Astronomical Research in the Southern Hemisphere under ESO programme ID 093.D-0286. SV gratefully acknowledges the support provided by Fondecyt reg. n. 1170518. CM also thanks the support provide by CONICYT through Beca Postdoctorado en el Extranjero convocatoria 2018 folio 74190045. DG gratefully acknowledges support from the Chilean Centro de Excelencia en Astrofísica y Tecnologías Afines (CATA) BASAL grant AFB-170002. DG also acknowledges financial support from the Dirección de Investigación y Desarrollo de la Universidad de La Serena through the Programa de Incentivo a la Investigación de Académicos (PIA-DIDULS). We would also like to thank the referee for his valuable comments.

REFERENCES

Barbuy B. et al., 2013, A&A, 559, A5
Barbuy B. et al., 2016, A&A, 591, A53
Barklem P. S. et al., 2005, A&A, 439, 129
Baumgardt H., Hilker M., 2018, MNRAS, 478, 1520
Beaulieu S. F., Freeman K. C., Kalnajs A. J., Saha P., Zhao H., 2000, AJ, 120, 855
Blanton M. R. et al., 2017, AJ, 154, 28
Bressan A., Marigo P., Girardi L., Salasnich B., Dal Cero C., Rubele S., Nanni A., 2012, MNRAS, 427, 127
Carretta E. et al., 2009, A&A, 505, 117
Carretta E., Bragaglia A., Gratton R. G., Recio-Blanco A., Lucatello S., D'Orazi V., Cassisi S., 2010a, A&A, 516, A55
Carretta E. et al., 2010b, ApJ, 714, L7
Carretta E., Lucatello S., Gratton R. G., Bragaglia A., D'Orazi V., 2011, A&A, 533, A69
Carretta E. et al., 2015, A&A, 578, A116
Cayrel R. et al., 2004, A&A, 416, 1117

Choi J., Dotter A., Conroy C., Cantiello M., Paxton B., Johnson B. D., 2016, ApJ, 823, 102
Choi J., Dotter A., Conroy C., Ting Y.-S., 2018, ApJ, 860, 131
Cohen R. E., Moni Bidin C., Mauro F., Bonatto C., Geisler D., 2017, MNRAS, 464, 1874
Cortés C. C., Minniti D., Villanova S., 2019, MNRAS, 485, 4502
D'Antona F., Vesperini E., D'Ercole A., Ventura P., Milone A. P., Marino A. F., Tailo M., 2016, MNRAS, 458, 2122
Da Costa G. S., Held E. V., Saviane I., Gullieuszik M., 2009, ApJ, 705, 1481
Dias B., Barbuy B., Saviane I., Held E. V., Da Costa G. S., Ortolani S., Gullieuszik M., Vásquez S., 2016, A&A, 590, A9
Dotter A., 2016, ApJS, 222, 8
Dotter A., Chaboyer B., Jevremović D., Kostov V., Baron E., Ferguson J. W., 2008, ApJS, 178, 89
Dotter A., Milone A. P., Conroy C., Marino A. F., Sarajedini A., 2018, ApJ, 865, L10
Eisenstein D. J. et al., 2011, AJ, 142, 72
Ernandes H., Barbuy B., Alves-Brito A., Friaça A., Siqueira-Mello C., Allen D. M., 2018, A&A, 616, A18
François P. et al., 2007, A&A, 476, 935
Fulbright J. P., 2000, AJ, 120, 1841
Gilmore G. et al., 2012, The Messenger, 147, 25
Gonzalez G., Vanture A. D., 1998, A&A, 339, L29
Gonzalez O. A., Rejkuba M., Zoccali M., Valenti E., Minniti D., Schultheis M., Tobar R., Chen B., 2012, A&A, 543, A13
Gratton R. G., Lucatello S., Bragaglia A., Carretta E., Momany Y., Pancino E., Valenti E., 2006, A&A, 455, 271
Gratton R. G. et al., 2007, A&A, 464, 953
Gratton R., Carretta E., Bragaglia A., Lucatello S., D'Orazi V., 2010, The Messenger, 142, 28
Gratton R. G., Johnson C. I., Lucatello S., D'Orazi V., Pilachowski C., 2011, A&A, 534, A72
Grieco V., Matteucci F., Pipino A., Cescutti G., 2012, A&A, 548, A60
Guarnieri M. D., Ortolani S., Montegriffo P., Renzini A., Barbuy B., Bica E., Moneti A., 1998, A&A, 331, 70
Harris W. E., 1996, AJ, 112, 1487
Johnson C. I., Pilachowski C. A., Simmerer J., Schwenk D., 2008, ApJ, 681, 1505
Johnson C. I., Rich R. M., Kobayashi C., Kunder A., Koch A., 2014, AJ, 148, 67
Kurucz R. L., 1970, SAO Special Report. p. 309
Lecureur A., Hill V., Zoccali M., Barbuy B., Gómez A., Minniti D., Ortolani S., Renzini A., 2007, A&A, 465, 799
Majewski S. R. et al., 2017, AJ, 154, 94
Marino A. F., Villanova S., Piotto G., Milone A. P., Momany Y., Bedin L. R., Medling A. M., 2008, A&A, 490, 625
Marino A. F. et al., 2011a, A&A, 532, A8
Marino A. F. et al., 2011b, ApJ, 731, 64
Mauro F. et al., 2014, A&A, 563, A76
Mészáros S. et al., 2015, AJ, 149, 153
Minniti D. et al., 2010, New A, 15, 433
Mucciarelli A., Lapenna E., Massari D., Ferraro F. R., Lanzoni B., 2015, ApJ, 801, 69
Muñoz C., Geisler D., Villanova S., 2013, MNRAS, 433, 2006
Muñoz C., Villanova S., Geisler D., Saviane I., Dias B., Cohen R. E., Mauro F., 2017, 605, A12, A&A, preprint (arXiv:1705.02684)
.Muñoz C. et al., 2018, 620, A96, A&A, preprint (arXiv:1809.04164)
Mura-Guzmán A., Villanova S., Muñoz C., Tang B., 2017, MNRAS, 474, 4541, preprint (arXiv:1711.03176)
Nandakumar G., Ryde N., Schultheis M., Thorsbro B., Jönsson H., Barklem P. S., Rich R. M., Fragkoudi F., 2018, MNRAS, 478, 4374
Ness M. et al., 2013, MNRAS, 430, 836
Neuforge-Verheecke C., Magain P., 1997, A&A, 328, 261
Origlia L. et al., 2011, ApJ, 726, L20
Pancino E. et al., 2017, A&A, 601, A112
Portail M., Gerhard O., Wegg C., Ness M., 2017, MNRAS, 465, 1621
Rain M. J., Villanova S., Munõz C., Valenzuela-Calderon C., 2019, MNRAS, 483, 1674
Reddy B. E., Tomkin J., Lambert D. L., Allende Prieto C., 2003, MNRAS, 340, 304
Reddy B. E., Lambert D. L., Allende Prieto C., 2006, MNRAS, 367, 1329
Sahu K. C. et al., 2006, Nature, 443, 534
Saviane I., da Costa G. S., Held E. V., Sommariva V., Gullieuszik M., Barbuy B., Ortolani S., 2012, A&A, 540, A27
Sneden C., 1973, ApJ, 184, 839
Tang B. et al., 2017, MNRAS, 465, 19
Tang B. et al., 2018, ApJ, 855, 38
Van der Swaelmen M., Barbuy B., Hill V., Zoccali M., Minniti D., Ortolani S., Gómez A., 2016, A&A, 586, A1
Venn K. A., Irwin M., Shetrone M. D., Tout C. A., Hill V., Tolstoy E., 2004, AJ, 128, 1177
Ventura P., D'Antona F., Di Criscienzo M., Carini R., D'Ercole A., Vesperini E., 2012, ApJ, 761, L30
Villanova S., Geisler D., 2011, A&A, 535, A31
Villanova S., Geisler D., Carraro G., Moni Bidin C., Muñoz C., 2013, ApJ, 778, 186
Zoccali M., Renzini A., Ortolani S., Bica E., Barbuy B., 2001, AJ, 121, 2638

This paper has been typeset from a TEX/LATEX file prepared by the author.